The Four-Step, Double-Autocatalytic Mechanism for Transition-Metal Nanocluster Nucleation, Growth, and Then Agglomeration: Metal, Ligand, Concentration, Temperature, and Solvent Dependency Studies

Eric E. Finney and Richard G. Finke*

Department of Chemistry, Colorado State University, Ft. Collins, Colorado 80523

Received April 22, 2007. Revised Manuscript Received October 11, 2007

The four-step, double-autocatalytic mechanism for transition-metal nanocluster nucleation, growth, and agglomeration described previously has been found to be more general; specifically, the four-step mechanism is shown to apply to the reduction of five transition metals that were examined—Pt, Ru, Ir, Rh, and Pd—under conditions where a high enough concentration of a strongly coordinating ligand is also present. Reaction temperature, metal concentration, solvent, and stirring rate do not change the reduction mechanism within experimental error and within the range of conditions studied herein. Changing the solvent from acetone to the higher dielectric constant solvent propylene carbonate does, however, change the product of metal reduction from solid bulk metal to soluble metal particles. Three alternative mechanisms (in addition to the 15 tested already) are ruled out, leaving the four-step double autocatalytic mechanism as the only mechanism to date that is able to fit the observed kinetic data. Additional support for the generality of the four-step mechanism is given by the identification of three additional literature systems for which the four-step mechanism is observed. Multiple other experiments and results are also described and then summarized in a Conclusions section.

Introduction

Two recent reports[1,2] provided reaction product and stoichiometry, transmission electron microscopy (TEM), X-ray photoelectron spectroscopy (XPS), nuclear magnetic resonance (NMR) spectroscopy, gas–liquid chromatography (GLC), and extensive experimental kinetic and numerical integration curve-fitting data for a four-step mechanism for transition-metal nanocluster formation and agglomeration from metal salts under reductive conditions such as H_2 (Scheme 1). The proposed minimalistic ("Ockham's razor") kinetic scheme and associated mechanism (Scheme 1) consists of[1,2] slow continuous nucleation, A → B (rate constant k_1), fast *autocatalytic* surface growth, A + B → 2B (rate constant k_2), bimolecular agglomeration, B + B → 2B (rate constant k_3), and a new, unprecedented *autocatalytic agglomeration step* between smaller particles (B) and what appear to be larger, more bulk-metal-like (C) particles, B + C → 1.5C (rate constant k_4)—although the exact nature of B and C remain to be elucidated via in-progress studies using extended X-ray absorption fine structure (EXAFS), X-ray absorption near-edge spectroscopy (XANES), small-angle X-ray scattering (SAXS), and other physical methods.[3] A novel feature of the mechanism is that two autocatalytic steps (steps 2 and 4 in Scheme 1) are present, that is, two steps in which a product is also a reactant. Reaction mechanisms including two autocatalytic steps are rare in the literature, prior examples being limited to the reactions of nitriles in high-temperature water,[4] the action of ATPase pumps,[5] oscillating reactions,[6a] and amplification of chirality.[6b] The four-step mechanism in Scheme 1 is a culmination of studies since 1994 investigating the mechanism of transition-metal nanocluster formation under reductive conditions.[7,8]

Scheme 1. Schematic Pictorial View Detailing the Four-Step, Double-Autocatalytic Mechanism for Transition-Metal Nanocluster Formation from Metal Salts under Reducing Conditions Such as H_2[a]

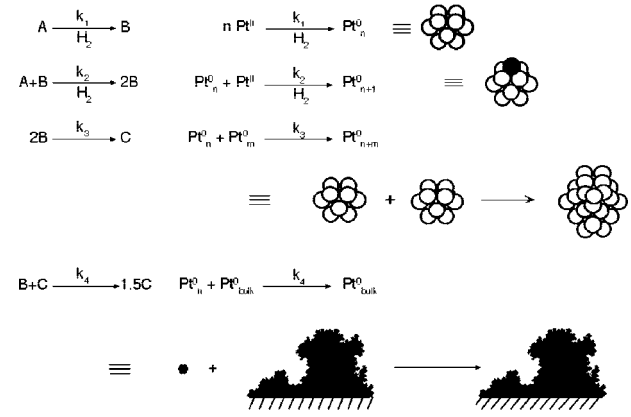

[a] The precise size and exact nature of the critical nucleus, Pt^0_n, as well as of B and C vs time remain to be elucidated.

* Corresponding author. E-mail: rfinke@lamar.colostate.edu.

(1) Besson, C.; Finney, E. E.; Finke, R. G. *J. Am. Chem. Soc.* **2005**, *127*, 8179.
(2) Besson, C.; Finney, E. E.; Finke, R. G. *Chem. Mater.* **2005**, *17*, 4925.
(3) (a) Autrey, T.; Linehan, J. C.; Fulton, J. L.; Özkar, S.; Finke, R. G. Experiments in progress. (b) Menard, L.; Frenkel, A. I.; Nuzzo, Finney, E. E.; Graham, C.; Alley, W. M.; Finke, R. G. Experiments in progress.
(4) Izzo, B.; Harrell, C. L.; Klein, M. T. *AIChE J.* **1997**, *43*, 2048.
(5) Weissmüller, G.; Bisch, P. M. *Eur. Biophys. J.* **1993**, *22*, 63.
(6) (a) Epstein, I. R.; Pojman, J. A. *An Introduction to Nonlinear Chemical Dynamics. Oscillations, Waves, Patterns and Chaos*; Oxford University Press: Oxford, 1998; p 98. (b) Kondepudi, D. K.; Asakura, K. *Acc. Chem. Res.* **2001**, *34*, 946.

10.1021/cm071088j CCC: $40.75 © 2008 American Chemical Society
Published on Web 02/16/2008

The primary system examined in our most recent kinetic and mechanistic work[1,2] is Pt(1,5-COD)Cl_2 under the specific conditions of 1.34 mM Pt(1,5-COD)Cl_2, 2.66 mM Bu_3N, 2.69 mM Proton Sponge (1,8-bis(dimethylamino)naphthalene, a strong, noncoordinating preferred base[9] used to scavenge the protons formed by H_2 reduction of Pt^{II}, Scheme 1), 1.65 M cyclohexene, and acetone as solvent, all initially under 40 psig of hydrogen. A typical, diagnostic—albeit unprecedented until recently[1,2]—kinetic curve is shown in Figure 1 in which a variable, ca. 0.4–3.0 h induction period is followed by the reaction "taking off" very suddenly after that in an almost step-function-like manner. The initially clear, colorless reaction solution changes to cloudy black just after the end of the induction period. TEM of a drop of the solution harvested 5 min after the end of the induction period reveals the presence of 4.0 ± 1.0 nm nanoclusters.[1,2] At the end of the reaction, agglomerated black bulk Pt^0 metal (verified by XPS) is visible in the solution, on the stir bar, and on the walls of the reaction tube—that is, a phase transition to bulk Pt^0 begins near the end of the induction period when hydrogenation begins suddenly.

A key result from the prior reports is that the larger, apparently bulk-metal-like particles, C, are the superior hydrogenation catalyst over the normally more active nanoclusters, B, due to a postulated particle-size-dependent fractional surface-coverage effect including an apparent particle-size-dependent metal–ligand bond dissociation energy (BDE).[1,2] Independent experimental evidence for a size-dependent surface coverage exists; for example, Leff et al. found that for Au clusters ligated with thiols the extent of surface coverage decreases with increasing cluster size,[10] as one might expect since smaller, highly curved nanoclusters are more readily covered by ligands than bulk metal, which has a relatively flat surface. Calculations of CO adsorbed on small Co clusters (containing 13–55 atoms) gave a similar trend of decreasing binding energy with increasing cluster size.[11,12] The existence of a greater number of more coordinatively unsaturated edge and terrace sites on nanoclusters vs bulk metal may be a factor in the increased ligand binding energy in nanoclusters. In 1992, Schmid reported differential scanning calorimetry (DSC) and extended X-ray absorption fine structure (EXAFS) studies that showed that Au−Au bond strengths in Au_{55} clusters are 15 kcal/mol greater than those in bulk Au metal.[13] In addition, N_2 bound to bulk Ni metal has a bond dissociation energy $\sim^1/_2$ that of

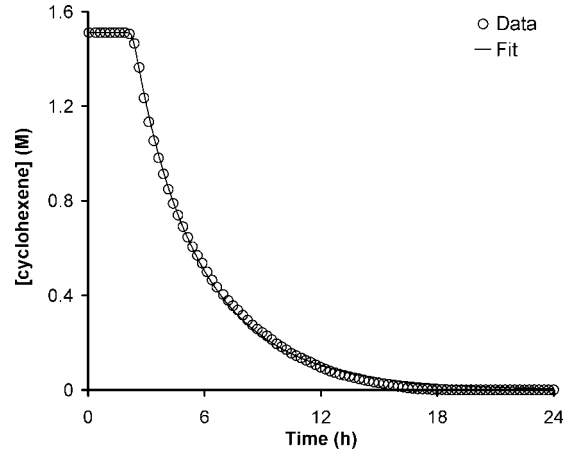

Figure 1. Typical kinetic curve for the reduction of Pt(1,5-COD)Cl_2, in the presence of 2 equiv of Proton Sponge and 2 equiv of Bu_3N, plus cyclohexene hydrogenation as a concomitant reporter reaction.[8] For clarity, only every fourth datum point is shown. The data are fit to the four-step mechanism shown in Scheme 1; note the excellent fit that results to this unusually shaped kinetic curve (residual = 0.012).

Ni_n(nanocluster)−N_2 bonds.[14] In short, the phenomenon of stronger metal–ligand bonds with decreasing particle size has precedent but was little appreciated in nanocluster chemistry until its effects in catalysis by B vs C (Scheme 1) were discovered in 2005.[1,2]

The prior studies of the reduction of Pt(1,5-COD)Cl_2[1,2] provided preliminary evidence that important variables in the four-step, double-autocatalytic mechanism in Scheme 1 include the initial metal precursor concentration, A (e.g., Pt(1,5-COD)Cl_2 in the prior work[1,2]), the temperature, and added nanocluster ligands/poisons such as tributylamine or pyridine.[1,2] However, none of these variables were explored in any detail. Key questions left unanswered by the prior work[1,2] include the following: (i) How general is the four-step, double-autocatalytic mechanism in Scheme 2? (ii) Does the addition of ligands affect the reduction mechanism, that is, can a reduction that follows the two-step mechanism (the first two steps of Scheme 1) be "forced" into the four-step mechanism by the addition of ligands, as our preliminary studies suggested might be the more general case?[1,2] (iii) How is the mechanism influenced by precursor concentration? (iv) How is the mechanism influenced by reaction temperature? Also, (v) are there major effects[15] of (always imperfect[15]) stirring on a reaction involving *two* autocatalytic steps? Reactions with even one autocatalytic step can be highly sensitive to such stirring effects.[15]

Herein we report studies showing the following: (i) The four-step mechanism is quite general to at least the five

(7) Lin, Y.; Finke, R. G. *J. Am. Chem. Soc.* **1994**, *116*, 8335.
(8) (a) Watzky, M. A.; Finke, R. G. *J. Am. Chem. Soc.* **1997**, *119*, 10382. (b) Widegren, J. A.; Aiken, J. D., III; Özkar, S.; Finke, R. G. *Chem. Mater.* **2001**, *13*, 312. (c) Hornstein, B. J.; Finke, R. G. *Chem. Mater.* **2004**, *16*, 139 (see also the addition/correction published in *Chem. Mater.* **2004**, *16*, 3972).
(9) Özkar, S.; Finke, R. G. *Langmuir* **2002**, *18*, 7653.
(10) Leff, D. B.; Ohara, P. C.; Heath, J. R.; Gelbart, M. W. *J. Phys. Chem.* **1995**, *99*, 7036.
(11) Reboredo, F. A.; Galli, G. *J. Phys. Chem. B* **2006**, *110*, 7979.
(12) (a) Karmazyn, A. D.; Fiorin, V.; King, D. A. *J. Am. Chem. Soc.* **2004**, *126*, 14273. (b) Nørskov, J. K.; Bligaard, T.; Logadottir, A.; Bahn, S.; Hansen, L. B.; Bollinger, M.; Bengaard, H.; Hammer, B.; Sljivancanin, Z.; Mavrikakis, M.; Xu, Y.; Dahl, S.; Jacobsen, C. J. H. *J. Catal.* **2002**, *209*, 275.
(13) Schmid, G. *Chem. Rev.* **1992**, *92*, 1709.
(14) Parks, E. K.; Nieman, G. C.; Kerns, K. P.; Riley, S. J. *J. Chem. Phys.* **1998**, *108*, 3731.
(15) (a) Stirring effects are known from Epstein's seminal work[15b] to have a dramatic effect on the level of reproducibility of systems involving autocatalytic reactions, A + B → 2B (i.e., where B is both a reactant and a product). The classic case in point is the chlorite−thiosulfate, ClO_2^-−$S_2O_3^{2-}$, "clock" reaction Epstein describes.[15b] He notes that: "Careful efforts to remove all the sources of variability among (repeat) experiments met with *total failure* (italics have been added). Despite elaborate schemes to ensure that all experiments were the same with regard to temperature, initial concentrations, exposure to light, vessel surface, age of solutions and mixing procedure, the reaction times still varied over a wide range" (b) Epstein, I. R. *Nature (London)* **1995**, *374*, 321.

metals studied under selected conditions (vide infra): platinum, ruthenium, iridium, rhodium, and palladium. (ii) The concentration and type of ligands present have a large an effect on the reduction mechanism (higher concentrations of strongly coordinating ligands favor the four-step mechanism). (iii) The reduction of Pd(1,5-COD)Cl_2 follows the four-step mechanism, but only when excess 1,5-COD is present; in the absence of excess 1,5-COD, the reduction occurs without an induction period. (iv) The number of steps of the reduction mechanism is independent of reaction temperature, metal concentration, and stirring rate. In addition, (v) the products of the metal reduction can be changed from bulk metal to nanoclusters by choice of solvent, rather than temperature and concentration as tentatively concluded previously, and (vi) changes in *nucleation* (rate constant k_1) are shown to have controlling effects on whether agglomerated/bulk-metal product is observed.[1,2] Also included is a section discussing additional literature systems found by us that exhibit the four-step, double-autocatalytic mechanism. The results are significant in establishing the broader generality, and defining the key variables, of the four-step, double-autocatalytic mechanism of transition-metal nanocluster formation under the common conditions of H_2 reduction of metal salts. At least at present, there is no alternative, kinetically verified mechanism for transition-metal nanocluster nucleation, growth, and agglomeration.

Experimental Section

General Considerations. All manipulations were carried out under air-free conditions using a Vacuum Atmospheres N_2 drybox maintained at ≤5 ppm O_2 as monitored by a Vacuum Atmospheres O_2 level monitor. Unless indicated otherwise, all commercially available solvents, compounds, and materials were used as received. Acetone (Burdick and Jackson, water content <0.2%) was purged with argon for 20 min and stored in the drybox. Propylene carbonate (Aldrich) was evacuated for 4 h before being stored in the drybox over activated 4 Å molecular sieves. Cyclohexene (Aldrich, 99%) and tributylamine (J.T. Baker Chemicals) were both purified by their separate distillation over sodium under argon followed by storage in the drybox. Hydrogen gas (General Air, 99.5%) was purified bypassing through a moisture trap, an O_2 cartridge, and an indicating O_2 trap (Trigon Technologies, Rancho Cordova, CA). The complexes [Ir(1,5-COD)Cl]$_2$ (99%), [Rh(1,5-COD)Cl]$_2$ (98%), Pt(1,5-COD)Cl_2 (99%), Pd(1,5-COD)Cl_2 (99%), and Ru(1,5-COD)Cl_2 (99%) were obtained from Strem Chemicals and used as received. Proton Sponge (1,8-bis(dimethylamino)naphthalene) (99%), silver tetrafluoroborate (99.9%), 4-(dimethylamino)pyridine (99.9%), and tetrabutylammonium chloride (≥97%) were obtained from Aldrich and stored in the drybox. Octanethiol (Aldrich, 98%) was taken into the drybox only when needed and then removed immediately after its use, as thiols are known poisons for the drybox catalyst. Pyridine (Aldrich, 99%) was distilled under vacuum and stored in the drybox over activated 4 Å molecular sieves. Stock solutions of tributylamine and pyridine were prepared and stored in the drybox; the tributylamine solution (42 mM) was prepared by mixing 0.1 mL (0.42 mmol) of tributylamine and 9.9 mL of acetone; the pyridine solution (18 mM) was prepared by diluting 73 μL (0.91 mmol) of pyridine to 50 mL with acetone.

Hydrogenations: Standard Conditions. Hydrogenation reactions were performed as previously described using our custom-built pressurized hydrogenation apparatus.[7] Briefly, the appropriate amount of the metal precursor salt was weighed into a 1-dram glass vial (3.6 μmol in a Standard Conditions hydrogenation). Proton Sponge was added to the vial (1 equiv for Ir^I and Rh^I and 2 equiv for Pt^{II}, Pd^{II}, and Ru^{II}). When added ligand was employed, the appropriate amounts of ligand or ligand stock solution plus solvent were added to make a 2.5 mL homogeneous solution. The resultant solution was added to a new 22 × 175 mm Pyrex borosilicate culture tube containing a new 5/8 × 5/16 in. Teflon-coated magnetic stir bar, and 0.5 mL of cyclohexene was added to the solution (resulting in a metal concentration of 1.2 mM in a Standard Conditions hydrogenation). The culture tube was placed in a Fischer–Porter (hereafter F-P) bottle, which was then sealed and brought out of the drybox. The bottle was placed in a mineral oil bath maintained at 22.0 ± 0.1 °C by a constant temperature recirculating water bath (VWR Scientific). The bottle was connected to the hydrogenation apparatus via its TFE-sealed Swagelock quick connects. Stirring was started, and the bottle was purged 13 times with hydrogen (15 s per purge) and stirred for an additional 1 min 45 s (total time elapsed 5 min). The pressure in the bottle was set to 40.0 ± 0.1 psig of H_2, $t = 0$ was noted, and data collection was initiated using an Omega PX-621 pressure transducer interfaced with a PC running LabVIEW 6.1.[7] Correction for the initial increase in acetone vapor pressure (when acetone was used as the solvent) was performed as described elsewhere[16] by independently measuring a curve (i.e., the initial increase in pressure) of a mixture of 2.5 mL of acetone and 0.5 mL of cyclohexene and then subtracting point by point that vapor pressure increase contribution from the kinetic data at early times.[16]

Data analysis was performed using nonlinear least-squares curve fitting to the analytic equation for the two-step mechanism[8a] (Microcal Origin version 7) or, for the three- or four-step mechanisms,[2] numerical integration via MacKinetics version 0.9.1b.[17] A good fit using MacKinetics corresponded to residuals of ≤0.02 as well as a visually close fit; residuals were typically between 0.007 and 0.01. The details of the fitting procedure have been described previously in detail, along with a discussion of the larger error bars intrinsic to fits of the four-step mechanism.[2]

Reduction of the in Situ Generated Platinum Complex, [Pt(1,5-COD)Cl(acetone)]$^+$[BF_4]$^-$. In the drybox, 1.9 mg of Pt(1,5-COD)Cl_2 (5.08 μmol) was dissolved in 2.5 mL of acetone to make a clear, colorless solution. This solution was added to a vial containing 1.0 mg of $AgBF_4$ (5.14 μmol, 1.01 equiv vs Pt); a white precipitate of AgCl immediately formed. The vial was capped and Parafilmed and was brought out of the drybox. The vial was centrifuged for 20 min at ~1600 rpm to settle the white precipitate to the bottom of the vial. The vial was then returned to the drybox, and the clear colorless liquid was decanted into a new culture tube. The white solid (AgCl, 0.7 mg, 100%) was weighed to ensure that the reaction went to completion. Attempts to isolate the complex for characterization failed. Next, 0.5 mL of cyclohexene was added to the culture tube, and hydrogenation was performed as described above. The acetonitrile solvated complex [Pt(1,5-COD)Cl-(CH_3CN)]$^+$[BF_4]$^-$ and its Pd analogue were prepared, isolated, and characterized (see Supporting Information); these results parallel well-known metal−solvate complex literature where the CH_3CN solvates are of greater stability than the acetone solvates.[18] However, the acetonitrile complex gives irreproducible results when hydrogenated.

GLC Studies Following the Evolution of Cyclooctane from the Hydrogenation of [Ir(1,5-COD)Cl]$_2$. A Standard Conditions reaction (with the exception that all quantities were doubled) was

(16) Widegren, J. A.; Aiken, J. D., III; Ozkar, S.; Finke, R. G. *Chem. Mater.* **2001**, *13*, 312.
(17) Leipold, W. S., III http://members.dca.net/leipold/mk/advert.html.
(18) Wendlandt, W. W.; Bear, J. L.; Horton, G. R. *J. Phys. Chem.* **1960**, *64*, 1289.

started using $[Ir(1,5\text{-COD})Cl]_2$ and 5 equiv of pyridine. Samples for GLC analysis were taken using the following procedure: the gas-regulator valve between the F-P bottle and the hydrogen tank was opened. Next, the top valve of the F-P bottle was opened to allow a continuous stream of H_2 through the F-P bottle and out of the top valve. An ~0.1 mL aliquot of the reaction solution was removed with a gastight syringe equipped with a 30 cm long needle, and the aliquot was placed in a 1 mL screwcap vial. The top valve of the F-P bottle was immediately closed. After waiting 10 s for the F−P bottle to become repressurized to ~40 psig of H_2, the valve to the hydrogen tank was closed. The entire operation took less than 1 min. The sample was immediately analyzed by GLC using a Hewlett-Packard HP-5890 equipped with a Supelco SPB-1 capillary column (30 m × 0.25 mm) and a flame ionization detector and interfaced to a PC running Galaxie software (Galaxie Chromatography Data System, version 1.7.403.22). The sampling parameters were as follows: initial temperature 50 °C, initial time 3 min, ramp rate 10 °C/min, final temperature 160 °C, final time 10 min, injector temperature 180 °C, detector temperature 200 °C. The results of the GLC experiment are described in the main text.

Higher Temperature Studies. These hydrogenations were performed as above, except the temperature of the recirculating water bath was raised to a higher temperature (from 30.0 to 80.0 °C; see Results and Discussion). The temperature of the solution in the F-P bottle was verified by placing a thermometer in a culture tube inside the F-P bottle that contained 3 mL of propylene carbonate. For these high-temperature reactions, the F-P bottle was kept in the oil bath for 3–5 min before purging with H_2 to allow the temperature of the solution to equilibrate with the temperature of the oil bath. At the highest temperature studied (80 °C), the cyclohexane formed during the reaction boiled (cyclohexane bp 80.7 °C) and recondensed at the top of the culture tube in the F-P bottle. This cyclohexane "distillation" resulted in a series of pressure spikes as measured by the pressure transducer. A representative example of this phenomenon is shown in the Supporting Information, Figure S1. However, the rate constants were obtained by fitting only the first half of the data[8a] (i.e., before too much of the "distillation" occurs), so that this phenomenon is not expected to have a significant impact on the calculations of the rate constants. As a control to test the reproducibility, the reactions were reproduced three times and resulted in the same observed rate constants each time.

Another Way To Judge the Quality of the Fit: The *F* Test. In the data sets which follow, the residual given by the MacKinetics program has been used to judge how closely the fit matches the data, lower values of *r* (along with a visually close fit) indicating a better fit. To provide an independent and more universal measure of the fit quality, we also employed the statistical *F* test. Details of this statistical technique are given elsewhere,[19] but the essence for the purposes of this paper is that the variances of the fit to the data and the fit were compared to determine whether the two sets of data are statistically equal. The *F* value is the measure of the similarities of the variances of the fit to the data—the closer that value is to 1, the more likely the data and fits are equal. For example, for the data in Figure 1 which follows, the fit to the four-step mechanism gives an *F* value of 1.000(6) at the 95% confidence level, indicating an excellent fit. The *F* value associated with the two-step mechanism fit is 0.825 at the 95% confidence level, indicating an inferior fit (Figure S2a in the Supporting Information shows the visually inferior fit of the two-step mechanism). The results of the *F* test for representative four-step fits in this study are tabulated in the Supporting Information, Table S1.

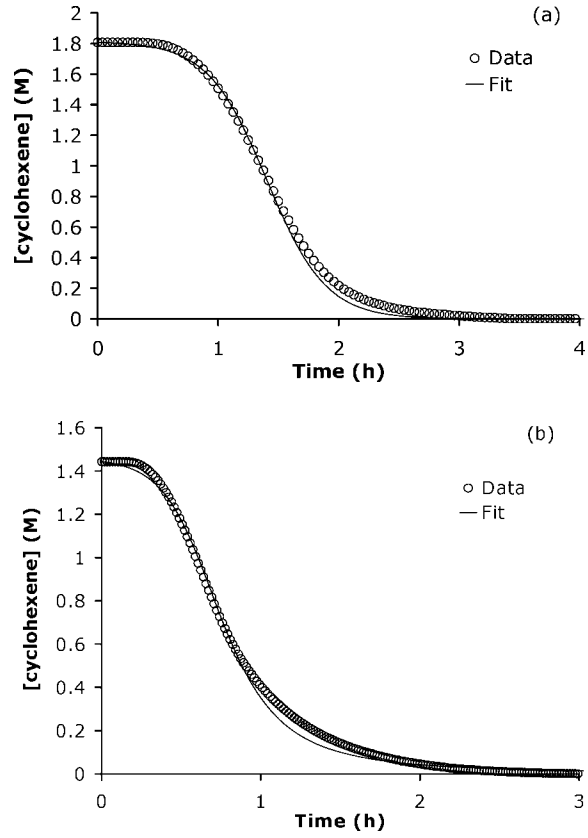

Figure 2. Kinetic curves for the reduction of $(Bu_4N)_5Na_3[(1,5\text{-COD})Ir{\cdot}P_2W_{15}Nb_3O_{62}]$ (a) in the absence of added ligand and (b) in the presence of 2 equiv of pyridine. The curve fit in (a) is to the two-step mechanism in Scheme 3 (with rate constants and indicated error bars $k_1 = 0.012(1)\ h^{-1}$ and $k_2 = 3.21(7) \times 10^3\ M^{-1}\ h^{-1}$), while the curve fit in (b) is to the three-step mechanism in Scheme 4 (with rate constants $k_1 = 0.063\ h^{-1}$, $k_2 = 5.4 \times 10^3\ M^{-1}\ h^{-1}$, and $k_3 = 1.8 \times 10^3\ M^{-1}\ h^{-1}$ and residual = 0.025). In (b), the fit misses some of the early and later parts of the curve, an indicator that the four-step mechanism is beginning to be a component (vide infra) of that particular reaction. Note the clear difference in the appearances of these curves to that shown in Figure 1. Error bars are reported for the two-step fit since the fit uses an analytic equation,[8a] while a residual is reported for the four-step fit since that fit is obtained using MacKinetics numerical integration.[1,2]

Results and Discussion

Kinetic Method Employed. It is important to understand how the kinetics of the multistep, self-assembly nanocluster formation reaction (eq 1) are monitored. The kinetic data are obtained indirectly, but powerfully and in real time, by the method first developed in a series of papers[7,8] dating back to 1994. This method employs the ability of the resulting metal^0 product, *the bulk-like metal (C) in the case of the four-step mechanism,*[1,2]to serve as a fast cyclohexene hydrogenation catalyst, eq 2—that is, the rate of the hydrogenation in eq 2 is fast relative to the rates of the reactions in eqs 1a−1d. The fast cyclohexene hydrogenation reporter reaction can therefore be used to follow the loss of H_2 via a computer-interfaced, high-precision (±0.1 psig) pressure transducer. The H_2 loss is, for convenience, converted to the equivalent cyclohexene loss (by the known 1 H_2:1 cyclohexene stoichiometry in Scheme 1), and then the rate constants for the nanocluster nucleation, growth, and agglomeration steps, k_1-k_4 in Scheme 1, are obtained[1,2,8] using the now well-documented pseudoelementary step method (vide infra).[7] This method—the addition of the fast

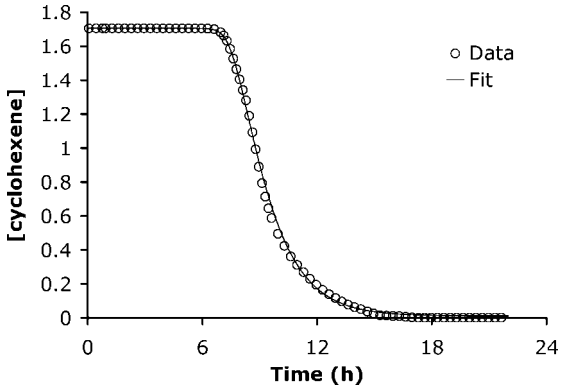

Figure 3. Kinetic curve for the reduction of 1.2 mM Pt(1,5-COD)Cl_2 with 2 equiv of Proton Sponge and the concomitant cyclohexene hydrogenation reporter reaction. For clarity in visualizing the fit, only every fourth datum point is shown. The curve fit is to the four-step, double-autocatalytic mechanism: $k_1 \approx 1 \times 10^{-7}$ h^{-1}, $k_2 \approx 1.6 \times 10^{3}$ M^{-1} h^{-1}, $k_3 \approx 1.7 \times 10^{2}$ M^{-1} h^{-1}, $k_4 \approx 9.1 \times 10^{2}$ M^{-1} h^{-1} (residual = 0.010). For a discussion of the precision and error limits on k_1-k_4, see the discussion elsewhere.[2]

catalytic reporter reaction (eq 2) to the slow steps that produce C (eqs 1c and 1d)—allows one to write eq 3 to make the needed connection between cyclohexene loss and the formation of C (the pseudoelementary step in this system is eq 3d).[7] The rate constants k_1-k_4 are then found by numerical integration curve-fitting and grid-search methods using MacKinetics.[17,20] Full details of the pseudoelementary step method,[7] the MacKinetics curve-fitting, and the grid-search methods employed are also documented in earlier papers.[2,7]

$$A \xrightarrow{k_1} B \qquad (1a)$$

$$A + B \xrightarrow{k_2} 2B \qquad (1b)$$

$$B + B \xrightarrow{k_3} C \qquad (1c)$$

$$B + C \xrightarrow{k_4} 1.5C \qquad (1d)$$

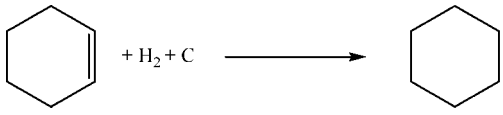

(2)

As briefly noted in the Introduction, the four-step, double-autocatalytic mechanism in Scheme 1 is a culmination of our studies investigating the mechanism of nanocluster formation from metal salts under reductive conditions such as H_2. For what follows, it will be important to be able to quickly and visually distinguish between the four-step mechanism (e.g., Figure 1, vide supra, or Figure 3, vide infra) from the two-step mechanism (Scheme 2 and Figure 2a) or three-step mechanism (Scheme 3 and Figure 2b).

Two immediate visual properties of the kinetic curves serve to distinguish the four-step mechanism from the two- and three-step mechanisms: (i) the sharp loss of cyclohexene after the induction period (the sudden "turn-on" mentioned above and shown in Figure 1) and (ii) the absence of an inflection point in the curve. These two qualitative features (which can be seen in Figure 1, but are absent from both of

Scheme 2

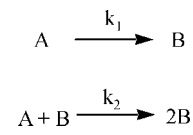

Scheme 3

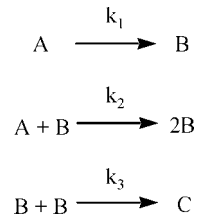

the curves in Figure 2) are instant indicators that the four-step, double-autocatalytic mechanism should be considered.

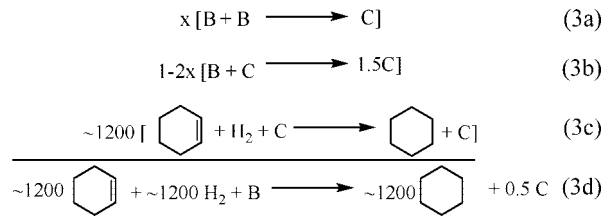

Herein we will search primarily for conclusions that are based on (i) whether or not the diagnostic curves of the four-step mechanism are seen and can be closely curve fit (i.e., with residuals ≤ 0.02), and (ii) conclusions involving comparisons between rate constants with differences $\geq 10^4$ in k_1 and $\geq 10^2$ in k_2-k_4 and, therefore, which should be valid.[1,2] This approach is necessary since minimization of the residual of the curve fit will in general be improved as one adds more parameters, so that, again, use of the *minimal* number of steps (i.e., the two- or three-step mechanism vs the four-step mechanism) is the "Ockham's Razor"[21] approach one must take.

Metal and Ligand Dependencies. The observed kinetic curves, and hence the resultant mechanism, proved to be *the most dependent on the metal being reduced and the added ligands/poisons*. Hence, the main results for the metal and ligand surveys are given first in what follows. These results are summarized in Table 1.

(19) Draper, N. R.; Smith, H. *Applied Regression Analysis*, 3rd ed.; Wiley: New York, 1998; Chapter 1.

(20) (a) Because of the difficult problem[20b] of searching a 5-dimensional space for five adjustable parameters (the four rate constants, k_1-k_4, plus the residual) for their global minimum, it is important to realize that the resultant k_2-k_4 rate constants are known only to within a factor of ca. 5–7-fold, while the k_1 is in what surface-mapping[2] shows is a very flat potential surface so that it is known to no better than ca. $10^{\pm 4}$ in some cases—even for the present state-of-the-art system[2] that may prove hard to better with its large amount of high precision ($\pm \leq 0.01$ psig of H_2 pressure; $\pm \leq 0.025\%$ out of 40 psig of H_2) data (typically 500–1500 data points and, hence, 100–300 data points per parameter).[2] (b) The following book on numerical analysis methods notes on p 387, in their chapter on minimization or maximization of functions, the fact that "Finding a global extremum is, in general, a very difficult problem": Press, W. H.; Teukolosky, S. A.; Vetterling, W. T.; Flannery, B. P. *Numerical Recipes in Fortran: The Art of Scientific Computing*, 2nd ed.; Cambridge University Press: New York, 1992.

(21) Hoffmann, R.; Minkin, V. I.; Carpenter, B. K. *Int. J. Philos. Chem.* **1997**, *3*, 3.

Table 1. Summary of Metal and Ligand Dependence on Reduction Mechanism[a]

entry	precursor complex	added ligand (equiv)	kinetic fit	time bulk metal observed
	Pt			
1	Pt(1,5-COD)Cl_2[b]	Bu_3N (2)	4-step	end of t_{ind}
2	Pt(1,5-COD)Cl_2	none	4-step	end of t_{ind}
3	[Pt(1,5-COD)Cl(acetone)][BF_4]	none	2-step	after cyclohexene hydrogenation
	Ru			
4	Ru(1,5-COD)Cl_2	none	4-step	end of t_{ind}
	Ir			
5	$(Bu_4N)_5Na_3$[(1,5-COD)Ir·$P_2W_{15}Nb_3O_{64}$][c]	pyridine (44)	4-step	N/O[d]
6	[Ir(1,5-COD)Cl]$_2$	none	2-step	after cyclohexene hydrogenation
7	[Ir(1,5-COD)Cl]$_2$	Bu_4NCl (1)	4-step	end of t_{ind}
8	[Ir(1,5-COD)Cl]$_2$	pyridine (1)	2-step	after cyclohexene hydrogenation
9	[Ir(1,5-COD)Cl]$_2$	pyridine (5)	4-step	end of t_{ind}
10	[Ir(1,5-COD)(CH_3CN)$_2$][BF_4]	none	2-step	after cyclohexene hydrogenation
11	[Ir(1,5-COD)(CH_3CN)$_2$][BF_4]	Bu_4NCl (2)	4-step	end of t_{ind}
12	[Ir(1,5-COD)(CH_3CN)$_2$][BF_4]	pyridine (1)	4-step	end of t_{ind}
	Rh			
13	[Rh(1,5-COD)Cl]$_2$	none	2-step	after cyclohexene hydrogenation
14	[Rh(1,5-COD)Cl]$_2$	Bu_4NCl (1)	4-step	N/O
15	[Rh(1,5-COD)Cl]$_2$	pyridine (50)	2-step	after cyclohexene hydrogenation
16	[Rh(1,5-COD)Cl]$_2$	4-(dimethylamino)pyridine (1)	2-step	N/O
17	[Rh(1,5-COD)Cl]$_2$	4-(dimethylamino)pyridine (10)	4-step	end of t_{ind}
18	[Rh(1,5-COD)(CH_3CN)$_2$][BF_4]	none	2-step	after cyclohexene hydrogenation
19	[Rh(1,5-COD)(CH_3CN)$_2$][BF_4]	Bu_4NCl (2)	4-step	end of t_{ind}
20	[Rh(1,5-COD)(CH_3CN)$_2$][BF_4]	pyridine (80)	2-step	N/O
21	[Rh(1,5-COD)(CH_3CN)$_2$][BF_4]	4-(dimethylamino)pyridine (10)	4-step	end of t_{ind}
	Pd			
22	Pd(1,5-COD)Cl_2	none	exponential	during purge cycle
23	Pd(1,5-COD)Cl_2	4-(dimethylamino)pyridine (20)	exponential	during purge cycle
24	Pd(1,5-COD)Cl_2	1,10-phenanthroline (1)	exponential	during purge cycle
25	Pd(1,5-COD)Cl_2	octanethiol (0.5)	exponential	during purge cycle
26	Pd(1,5-COD)Cl_2	1,5-COD (20)	4-step	end of t_{ind}

[a] All reactions are in acetone at room temperature. [b] From ref 1. [c] From ref 8c. [d] N/O = not observed.

Platinum. Reduction of Pt(1,5-COD)Cl_2 in the presence of 2 equiv of tributylamine was the first system for which the four-step mechanism was observed (Table 1, entry 1);[1,2] a typical kinetic curve is shown back in Figure 1.[2] As a control experiment, Pt(1,5-COD)Cl_2 was reduced in the absence of Bu_3N, with the expectation that the two-step mechanism would be observed. Interestingly, this latter reduction still follows the four-step mechanism (Figure 3), with an excellent fit to the observed data. Attempted curve fits to the two- and three-step mechanisms, and their associated rate constants, are given in the Supporting Information, Figure S2; they are clearly inferior to the fit with the four-step, double-autocatalytic mechanism. In fact, the four-step mechanism is needed to fit the data for the reduction of Pt(1,5-COD)Cl_2 over a range of reaction temperatures and metal concentrations (vide infra). It appears, therefore, that the 2 equiv of Cl^- from the precursor complex alone is sufficient to ligate/poison the Pt^0_n nanoclusters to the point that the four-step mechanism is necessary to fit the data.

As a control to see whether both Cl^- ligands present in Pt(1,5-COD)Cl_2 are necessary to bring about the four-step mechanism in the Pt complex, the solvated complex [Pt(1,5-COD)Cl(acetone)]$^+$[BF_4]$^-$ was prepared *in situ* in acetone and reduced under H_2 (Table 1, entry 2). The data, shown in Figure 4, are well fit by the two-step mechanism, not the four-step mechanism as seen for Pt(1,5-COD)Cl_2. Rather clearly, 1 equiv of Cl^- is insufficient to force the four-step mechanism for Pt.

A very interesting point in comparing the Pt(1,5-COD)Cl_2 + 2 equiv Proton Sponge system (Figure 3) vs the [Pt(1,5-COD)Cl(acetone)$^+$][BF_4]$^-$ + 2 equiv Proton Sponge system (Figure 4) is that it appears that the difference of just one additional Cl^- triggers a change from the two- to four-step

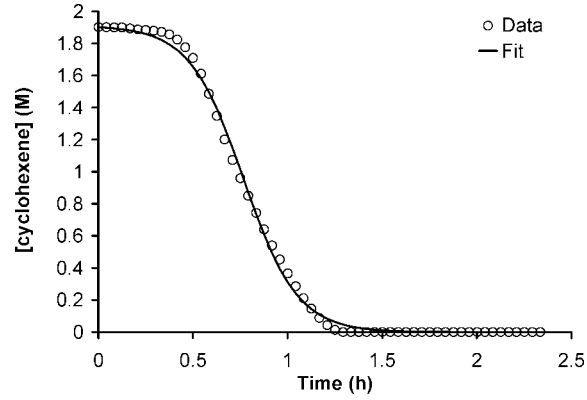

Figure 4. Kinetic curve for the reduction of *in situ* generated 1.2 mM [Pt(1,5-COD)Cl(acetone)]$^+$[BF_4]$^-$ with 1 equiv of Proton Sponge and the concomitant cyclohexene hydrogenation. The curve fit is to the two-step mechanism: $k_1 = 0.015(2)\ h^{-1}$; $k_2 = 6.3(2) \times 10^3\ M^{-1}\ h^{-1}$, meaning that removal of one Cl^- from Pt(1,5-COD)Cl_2 to give [Pt(1,5-COD)Cl(acetone)]$^+$[BF_4^-] has changed the mechanism from the four-step mechanism with C as the catalyst to primarily the two-step mechanism with B as the catalyst.

mechanism (i.e., triggers agglomeration). Initially, one might have expected the opposite—that more Cl^- might lead to better stabilized nanoclusters. But, additional salt (i.e., the Proton Sponge−H^+Cl^- reaction byproduct) can apparently compact the Debye double layer surrounding the clusters, allowing closer cluster–cluster contact and, ultimately, agglomeration.[22] A look at the rate constants for these two- vs four-step systems is actually more informative. In addition to turning on measurable k_3 and k_4 values ($1.7 \times 10^2\ M^{-1}\ h^{-1}$ and $9.1 \times 10^2\ M^{-1}\ h^{-1}$, respectively, vs ~0 for these in the two-step mechanism), the main difference is that the nucleation rate is slower in the four-step mechanism, even

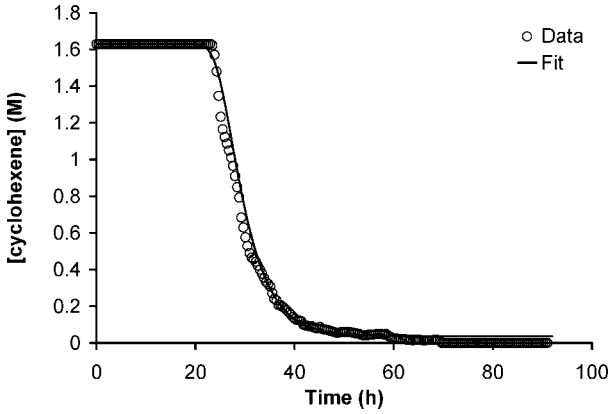

Figure 5. Kinetic curve for the reduction of 1.2 mM Ru(1,5-COD)Cl_2 with 2 equiv of Proton Sponge in the absence of ligand. The curve fit is to the four-step mechanism: (a) $k_1 \approx 2 \times 10^{-7}$ h^{-1}, $k_2 \approx 470$ M^{-1} h^{-1}, $k_3 \approx 46$ M^{-1} h^{-1}, $k_4 \approx 340$ M^{-1} h^{-1} (residual = 0.030). For clarity, only 1 out of every 10 datum points is shown.

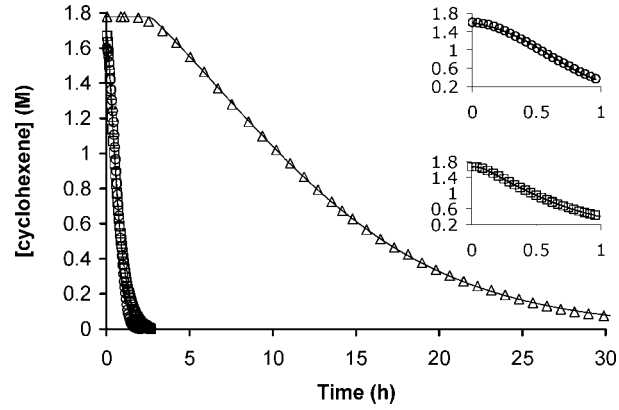

Figure 6. Kinetic curves for the reduction of 0.6 mM [Ir(1,5-COD)Cl]$_2$ (1.2 mM Ir) in the absence of added ligand (circles), in the presence of 1 equiv of Bu_4NCl (almost hidden squares), and in the presence of 5 equiv of pyridine (triangles, the slow reaction that ends at ~30 h). One equivalent of Proton Sponge is present in each reaction. The insets show the induction periods for the reduction of [Ir(COD)Cl]$_2$ with no ligand (circles, top inset) and with 1 equiv of Bu_4NCl (squares, bottom inset). The curve fits are to the two-step mechanism fit (no ligand), $k_1 = 0.28(2)$ h^{-1}, $k_2 = 3.6(1) \times 10^3$ M^{-1} h^{-1}, and to the four-step mechanism for the data with Bu_4NCl and pyridine−Bu_4NCl, $k_1 \approx 10$ h^{-1}, $k_2 \approx 8.5 \times 10^3$ M^{-1} h^{-1}, $k_3 \approx 4.1 \times 10^3$ M^{-1} h^{-1}, $k_4 \approx 3.0 \times 10^3$ M^{-1} h^{-1} (residual = 0.004), and pyridine, $k_1 \approx 2 \times 10^{-7}$ h^{-1}, $k_2 \approx 4.6 \times 10^3$ M^{-1} h^{-1}, $k_3 \approx 18$ M^{-1} h^{-1}, $k_4 \approx 200$ M^{-1} h^{-1} (residual = 0.005). For clarity, only 1 out of every 4 datum points is shown for the pyridine data. As before, error bars are reported for the two-step fit since the fit uses an analytic equation,[8a] while a residual is reported for the four-step mechanism fits obtained via MacKinetics numerical integration.[1,2]

given the $10^{\pm 4}$ error bars associated with k_1 in the four-step mechanism, $k_1 \approx 10^{-7}$ h^{-1} vs $k_1 = 10^{-2}$ h^{-1} in the two-step system. Restated, it is really *fewer nuclei*, and the resultant larger nanoclusters from largely unchanged growth ($k_2 = 6.3 \times 10^3$ M^{-1} h^{-1} for the two-step system vs $k_2 \approx 1.6 \times 10^3$ M^{-1} h^{-1} for the four-step system) that, in turn, lead to more agglomeration. *That is, the nucleation step is largely controlling the subsequent agglomeration.* This example nicely illustrates how, without knowledge of the nucleation kinetics, erroneous interpretation of why greater agglomeration results would be hard to avoid.

Ruthenium. The ruthenium complex Ru(1,5-COD)Cl_2 was reduced under H_2 in the absence of poison in acetone at room temperature (Figure 5). Reduction of this complex showed the same kinetics as the platinum dichloride complex; that is, 2 equiv of Cl^- is a sufficient amount of coordinating ligand to make the reduction follow the four-step mechanism. The significance of this result is that it provides immediate evidence that the four-step mechanism is applicable to metals other than platinum.

We tried to prepare the solvated ruthenium complex, [Ru(1,5-COD)Cl(CH_3CN)]$^+$[BF_4]$^-$, for study, but this was unsuccessful, as was the preparation of [Ru(1,5-COD)Cl(acetone)]$^+$[BF_4]$^-$. The difficulties inherent in the preparation of solvated Ru complexes have been previously documented.[23]

Iridium. Reduction of Ir^I to form nanoclusters has been extensively studied;[7,8] the B + B → C agglomeration step of the nanoclusters (B) when ligands such as pyridine are added (Scheme 2) has also been investigated.[8c] In the present work, [Ir(1,5-COD)Cl]$_2$ was reduced in acetone alone and in the presence of added ligands, namely chloride and the known nanocluster poison pyridine.[8c] Bulk Ir^0 metal proved to be the only product in both cases. In the absence of added ligands, the reduction followed the two-step mechanism (Figure 6, circles), as seen previously.[24] When 1 equiv of chloride was added in the form of Bu_4NCl to make 2 equiv of total Cl^- present vs Ir, the four-step mechanism was needed to fit the data (Figure 6, squares). Five equivalents of pyridine was also enough ligand to "force" the reduction into the four-step, double-autocatalytic mechanism (Figure 6, triangles). One equivalent of pyridine, however, is not enough to change the mechanism; the two-step mechanism was sufficient to fit the data (Supporting Information, Figure S3). In short, with either 2 total equiv of Cl^- or 5 equiv of added pyridine, the reduction of Ir^I is forced into the four-step mechanism. A small k_1 ($\approx 10^{-7}$ h^{-1}) is again apparent for the added pyridine system (albeit not for the added Cl^- system, $k_1 \sim 10$ h^{-1}, a result which may reflect the large error in the k_1 value[1,2]).

The same result was seen with the solvated complex [Ir(1,5-COD)(CH_3CN)$_2$]$^+$[BF_4]$^-$: in the absence of added ligand/poison, the two-step mechanism was able to fit the data, but the addition of either 2 equiv of Cl^- or 1 equiv of pyridine was sufficient to change the mechanism so that the four-step mechanism was required to fit the data (Supporting Information, Figure S4).

Recent results in our laboratory have suggested that the addition of pyridine may poison the cyclohexene hydrogenation reporter reaction to the point that it becomes ineffective in reporting the kinetics of nanocluster formation.[25] To see whether this is the case in the current system of [Ir(1,5-COD)Cl]$_2$ with 5 equiv of pyridine, we performed two control experiments. In the first, the concentration of cyclo-

(22) Evans, D. F.; Wennerström, H. *The Colloidal Domain*, 2nd ed.; Wiley-VCH: New York, 1999.
(23) Widegren, J. A.; Weiner, H.; Miller, S. M.; Finke, R. G. *J. Organomet. Chem.* **2000**, *610*, 112.
(24) Özkar, S.; Finke, R. G. *J. Am. Chem. Soc.* **2005**, *127*, 4800.
(25) Ott, L. S.; Finke, R. G. *Chem. Mater.* **2008**, in press.

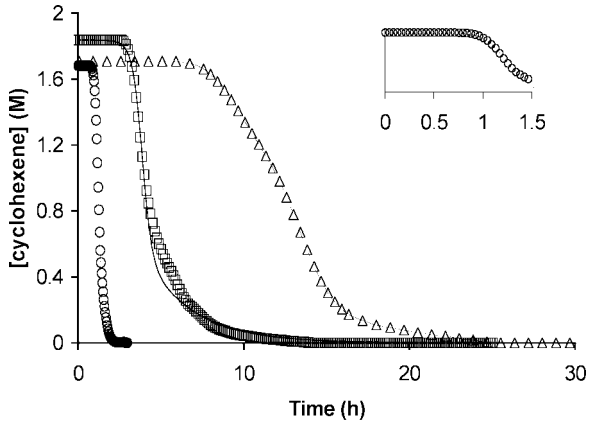

Figure 7. Kinetic curves for the reduction of 0.6 mM $[Rh(1,5\text{-}COD)Cl]_2$ (1.2 mM Rh) and 1 equiv of Proton Sponge in the absence of ligands (circles, the faster reaction that ends at ~3 h), in the presence of 1 equiv of Bu_4NCl (squares), and in the presence of 50 equiv of pyridine (triangles, the slower reaction that ends at ~25 h). The inset shows the induction period and fit for the reduction of $[Rh(1,5\text{-}COD)Cl]_2$ with no ligand (circles). The fits in the curves with no added ligand and with pyridine are to the two-step mechanism; with no ligand: $k_1 = 7(3) \times 10^{-4}$ h^{-1}, $k_2 = 6.0(4) \times 10^3$ M^{-1} h^{-1}; with 50 equiv of pyridine: $k_1 = 3.9(2) \times 10^{-4}$ h^{-1}, $k_2 = 4.8(5) \times 10^2$ M^{-1} h^{-1}. The fit to the curve with added Bu_4NCl is to the four-step mechanism: $k_1 \approx 6 \times 10^{-6}$ h^{-1}; $k_2 \approx 2.9 \times 10^3$ M^{-1} h^{-1}; $k_3 \approx 310 \times 10^3$ M^{-1} h^{-1}; $k_4 \approx 690 \times 10^3$ M^{-1} h^{-1} (residual = 0.010). Error bars, not a residual, are reported for the two-step fit since the fit uses an analytic equation,[8a] not MacKinetics numerical integration.[1,2] For clarity, only 1 out of 4 datum points is shown.

hexene was changed from the standard 1.65 M to 0.825 and then 3.30 M, that is, to one-half and then twice the standard concentration. These changes in cyclohexene concentration did not change the kinetics of the reaction, indicating that the nanocluster formation reaction remains zero-order in cyclohexene over this concentration range. In the second control experiment, described in a later section, the evolution of cyclooctane from the $[Ir(1,5\text{-}COD)Cl]_2$ complex was measured using gas–liquid chromatography. The rate constants from that measurement were the same within experimental error as those determined from the cyclohexene hydrogenation reporter reaction, indicating that the reporter reaction is indeed accurately reporting the kinetics of nanocluster formation for this system.

Rhodium. It was expected that the behavior of rhodium would be similar to that of iridium, the two metals being in the second and third rows of the same group;[26] however, this proved to be the case only for the addition of chloride. When $[Rh(1,5\text{-}COD)Cl]_2$ was reduced under H_2 in the absence of added ligands to form bulk Rh^0 metal as the final product, the two-step mechanism fit the data well (Figure 7, circles). Like the Ir system above, 1 equiv of added chloride (i.e., 2 equiv of total Cl^-) was sufficient so that the four-step mechanism was needed to fit the data (Figure 7, squares). However, unlike the Ir^I reduction case, the addition of pyridine did *not* change the mechanism to even the three-step mechanism; in fact, even 50 equiv of pyridine did not change the two-step mechanism. The reaction was significantly slowed compared to the reduction of $[Rh(1,5\text{-}COD)Cl]_2$ alone, but the kinetics still followed the two-step mechanism (Figure 7, triangles).

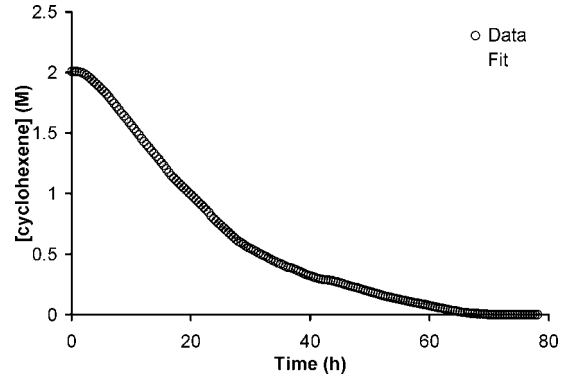

Figure 8. Kinetic curve for the reduction of 0.6 mM $[Rh(1,5\text{-}COD)Cl]_2$ (1.2 mM Rh) with 1 equiv of Proton Sponge in the presence of 10 equiv of 4-(dimethylamino)pyridine. The curve is best fit by the four-step mechanism: $k_1 \approx 0.3$ h^{-1}, $k_2 \approx 250$ M^{-1} h^{-1}, $k_3 \approx 9.7$ M^{-1} h^{-1}, $k_4 \approx 82$ M^{-1} h^{-1} (residual = 0.010). For clarity, only 1 out of every 10 datum points is shown.

In light of the above results, pyridine was replaced with a stronger base, namely 4-(dimethylamino)pyridine (pK_a of the conjugate acid = 9.7 vs 5.2 for pyridine), the prediction being that the stronger basicity (and hence stronger σ-donor ability) of this ligand would make it a more effective ligand for the second-row metal, Rh, with its weaker (than Ir) metal–ligand bond energy. Indeed, when 10 equiv of 4-(dimethylamino)pyridine were added to the reaction solution, the four-step mechanism became necessary to fit the kinetic curve (Figure 8). However, with only 1 equiv, the two-step mechanism was still sufficient to fit the data.

Similar results were obtained using the solvated complex $[Rh(1,5\text{-}COD)(CH_3CN)_2]^+[BF_4]^-$ (Supporting Information, Figures S5 and S6)—the addition of 2 equiv of Cl^- changed the mechanism from the two-step to the four-step mechanism, similar to the solvated Ir complex, but even 80 equiv of pyridine were unable enforce the four-step mechanism. However, using 10 equiv of the stronger base 4-(dimethylamino)pyridine did yield the four-step mechanism in the reduction of $[Rh(1,5\text{-}COD)(CH_3CN)_2]^+[BF_4]^-$ under H_2.

In short, the donor strength, as well as the concentration, of the added ligand and the nature of the metal (e.g., second row vs third row) are important in determining which mechanism the reduction will follow. More generally, it appears that high metal–ligand bond energies, plus sufficient concentrations of ligand to ensure bonding to the nanocluster, are crucial for enforcing the four-step mechanism. The resultant slowing of the k_1 nucleation step appears to be one key to inducing the formation of larger nanoclusters that agglomerate more readily, perhaps due to their weaker metal–ligand bond energies, as already discussed.[1,2]

Palladium. The reduction of $Pd(1,5\text{-}COD)Cl_2$ using our Standard Conditions began immediately without an induction period (Figure 9); the curve has the appearance of the four-step mechanism with the induction period removed. More specifically, the induction period was extremely short; the clear yellow $Pd(1,5\text{-}COD)Cl_2$ solution changed to black

(26) The second- and third-row metals are well known to have properties that are similar to each other and different from the first-row metals; this is a consequence of the lanthanide contraction. See for example: Miessler, G. L.; Tarr, D. A. *Inorganic Chemistry*; 3rd ed.; Prentice Hall: Upper Saddle River, NJ, 2004, Chapter 2.

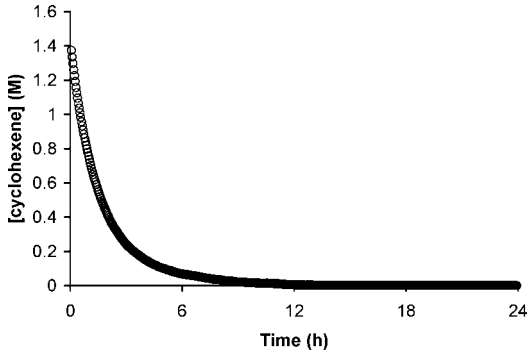

Figure 9. Kinetic curve for the reduction of 1.2 mM Pd(1,5-COD)Cl_2, and concomitant cyclohexene hydrogenation, in the presence of 2 equiv of Proton Sponge in acetone at room temperature.

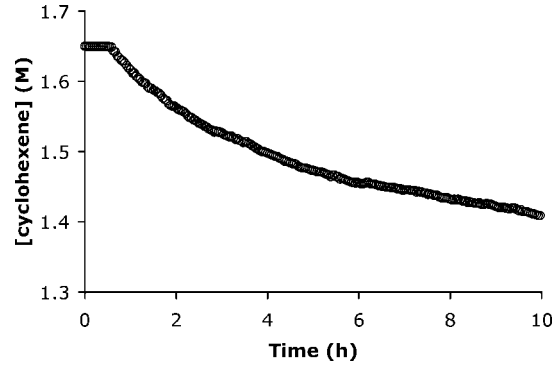

Figure 10. Kinetic curve for the reduction of Pd(1,5-COD)Cl_2 in the presence of 20 equiv of 1,5-COD in acetone. The fit to the first 10 h is to the four-step mechanism: $k_1 \approx 0.3\ h^{-1}$; $k_2 \approx 8.1 \times 10^3\ M^{-1}\ h^{-1}$; $k_3 \approx 11\ M^{-1}\ h^{-1}$; $k_4 \approx 0.75\ M^{-1}\ h^{-1}$; the residual is 0.094.

during the 5 min H_2 purge cycle of the Fischer–Porter bottle. Attempts to produce an induction period failed even on addition of the strongly coordinating ligands 4-(dimethylamino)pyridine (20 equiv) and 1,10-phenanthroline (1.0 equiv; this ligand has been implicated as a stabilizer in Moiseev's giant Pd clusters[27] and has recently been found by our group to be an effective nanocluster poison[28]). Even the common heterogeneous catalyst poison octanethiol failed to produce an induction period (0.5 equiv; this ligand has also been shown to poison/stabilize Pd nanoclusters[29]). The effect of all three added ligands was the same: they each slowed the hydrogenation of cyclohexene but did not introduce an induction period into the reduction; the general shape of the curve in Figure 9 was retained (Figure S7 of the Supporting Information).

Because it is important to find conditions where a slower, more kinetically controlled nucleation and growth of Pd^0_n occurs, other ligands were examined. The addition of 20 equiv of 1,5-COD did provide an induction period of ~0.6 h to the reduction (Figure 10). Visual inspection reveals the sharp "turn-on" and lack of inflection point in this short portion of the curve; these qualities indicate that the reduction follows the four-step mechanism as did a fit to the four-step mechanism (Figure 10). Note that the nucleation rate is still relatively large, $k_1 \approx 0.3\ h^{-1}$.

The addition of 20 equiv of 1,5-COD did not yield more stable nanoclusters, however. At the end of the induction period, the solution changed from clear and yellow to gray and then to clear and colorless with bulk metal present almost instantaneously. The change occurred so quickly that there was insufficient time to harvest a sample of the gray solution for TEM analysis.

Putting all of the observations up to this point together, some conclusions about the generality of the double autocatalytic mechanism are apparent. First, the four-step, double-autocatalytic mechanism appears general to the metals studied herein, Pt, Ru, Ir, Rh, and Pd, at least under the conditions examined. Second, sufficient amounts of a strongly coordinating ligand are crucial to "turning on" the four-step mechanism. Third, the nature of the metal is significant; for example, second row metals with weaker metal–ligand bonds require more basic ligands to enforce the four-step mechanism. Fourth, 2 equiv of chloride ion is a sufficient amount of coordinating ligand to turn on the four-step mechanism in all of the metals studied other than Pd, while 1 equiv is not.

The behavior of ligands other than chloride is more complex, as seen in the experiments reducing Ir^I and Rh^I in the presence of pyridine. Pyridine binds tightly enough to Ir to poison it when present in 5 equiv, but not even 50 equiv of pyridine can ligate/poison Rh to the point that the four-step mechanism is needed to fit the data—the two-step mechanism is sufficient even when 50 equiv of pyridine is present. However, the more basic 4-(dimethylamino)-pyridine ligand does induce the four-step mechanism for Rh, although 10 equiv of this more coordinating ligand are required. The effect of the ligands on the nucleation rate is relevant to these observations as are nanocluster size effects on the inherent metal–ligand bond energies; see the Supporting Information and data in Figure S8.

In the case of Pd(1,5-COD)Cl_2, the reduction takes place immediately upon exposure to H_2. Addition of excess 1,5-COD gives the reduction an observable induction period and shows that the four-step mechanism is operative in this case. A 1,5-COD dissociation equilibrium is implied, eq 4, but has not been unequivocally demonstrated. Note again that the four-step mechanism is followed.

$$Pd(1,5\text{-COD})Cl_2 + 2\text{solvent} \rightleftharpoons PdCl_2(\text{solvent})_2 + 1,5\text{-COD} \quad (4a)$$

$$PdCl_2(\text{solvent})_2 + H_2 \rightarrow \rightarrow Pd^0 + 2H^+Cl^- \quad (4b)$$

In light of the finding that with excess 1,5-COD the Pd complex is reduced under the four-step mechanism, the original data obtained in the absence of excess 1,5-COD was fit to the four-step mechanism to quantitate the kinetics of that fast reduction. The fit for Pd(1.5-COD)Cl_2, shown in the Supporting Information (Figure S9), gives a k_1 value of 20, a factor of $\sim 10^8$ greater (with a $10^{\pm 4}$ error[1,2]) than the

(27) (a) Vargaftik, M. N.; Kozitsyna, N. Y.; Cherkashina, N. V.; Rudyi, R. I.; Kochubei, D. I.; Novgorodov, B. N.; Moiseev, I. I. *Kinet. Catal.* **1998**, *39*, 806. (b) Starchevsky, M. K.; Hladiy, S. L.; Pazdersky, Y. A.; Vargaftik, M. N.; Moiseev, I. I. *J. Mol. Catal. A: Chem.* **1999**, *146*, 229.

(28) Hagen, C. M.; Vieille-Petit, L.; Laurenczy, G.; Süss-Fink, G.; Finke, R. G. *Organometallics* **2005**, *24*, 1819.

(29) (a) Brust, M.; Walker, M.; Bethell, D.; Schiffrin, D. J.; Whyman, R. *J. Chem. Soc., Chem. Commun.* **1994**, 801. (b) Zelakiewicz, B. S.; Lica, G. C.; Deacon, M. L.; Tong, Y. *J. Am. Chem. Soc.* **2004**, *126*, 10053.

k_1 value for the reduction of Pt(1,5-COD)Cl_2. It should be noted that while these values could conceivably be the same within the large, $10^{\pm 4}$ experimental error for each k_1, visual inspection of the curves in Figure 3 (for the reduction of Pt(1,5-COD)Cl_2) and Figure 9 (for the reduction of Pd(1,5-COD)Cl_2) strongly suggests that these rate constants are *not* the same and that k_1 for Pd^{2+} is significantly greater than k_1 for Pt^{2+}.

Indeed, the fast, kinetically *un*controlled reduction of Pd(1,5-COD)Cl_2 greatly counters the ≥0.4 h induction period for the reduction of Pt(1,5-COD)Cl_2. The reaction conditions—precursor, temperature, concentration, stirring rate—are the same for both complexes; the only difference is the metal (Pd^{2+} vs Pt^{2+}). The *aqueous* solution reduction potentials of Pd^{2+} and Pt^{2+} are similar: 0.99 V for Pd^{2+} and ca. 1.2 V for Pt^{2+}.[30] Hence, the difference in Pd^{2+} and Pt^{2+} reductions would appear to be primarily kinetic as opposed to thermodynamic in origin. Marcus theory considerations imply to us that a larger Pt vs Pd intrinsic barrier (reflecting larger Pt−ligand vs Pd−ligand BDEs) is very likely involved. Overall, the bottom line here is that nucleation is, again, a key.

It is worth noting in this regard that the nucleation steps for nanocluster formation are not well understood, even for the best studied polyoxoanion-stabilized $Ir^0_{\sim 300}$ nanocluster system.[8a] For example, metal hydrides[31] may be more important than the (controversial[32]) idea of metal(0) atoms as intermediates. The data above imply that the nucleation steps may be different when different conditions are used (e.g., when the metal or ligands are changed). Deeper investigation into nanocluster nucleation is needed and is in progress.[33]

Dependence on Other Variables for the Prototype Pt(1,5-COD)Cl_2 and [Ir(1,5-COD)Cl]$_2$ Reductions. Previously, we found that by changing reaction conditions (namely precursor concentration, reaction temperature, and solvent), we were able to tune the system to prepare either $Pt(0)_n$ nanoclusters or bulk metal.[1,2] Two questions arise from this result: (i) Do these changes in reaction conditions induce mechanistic changes, that is, will variations in these conditions change the number of steps necessary to fit the data? (ii) ¦What reaction conditions have the greatest influence over the product of the reaction (nanoclusters vs bulk metal)? To probe these questions, the reductions of Pt(1,5-COD)Cl_2 and [(Ir(1,5-COD)Cl]$_2$ were carried out several times while changing separately the reaction temperature, the initial metal concentration, the solvent, and the stirring rate, to determine what effect, if any, these variables have on the reduction of the metals.

Temperature Effects. The effect of temperature on the reduction mechanism of Pt(1,5-COD)Cl_2 and [Ir(1,5-COD)Cl]$_2$ was studied using a reaction temperature range of 22–80 °C and an initial metal concentration of 1.2 mM (i.e., the Standard Conditions concentration). Because of the relatively low boiling point of acetone (56 °C), the higher boiling solvent propylene carbonate (bp 242 °C) was used for these studies. Control experiments verified that the change of solvent from acetone to propylene carbonate did not affect the number of steps in the mechanism needed to fit the data (Supporting Information, Figures S10 and S11), showing that the same mechanism results when either acetone or propylene carbonate is used as the solvent. The results, listed in Table 2 for Pt^{II} reduction and Table 3 for Ir^{I} reduction, show that in the wide range of temperatures studied the temperature at which the reduction takes place has no effect on the number of steps in the mechanism—reduction of Pt(1,5-COD)Cl_2 requires all four steps to fit the kinetic curves, while reduction of [Ir(1,5-COD)Cl]$_2$ requires only the two-step mechanism. Although it is tempting to draw correlations between the calculated rate constants and the temperatures, the high experimental error that is inherent in the calculated rate constants for the four-step mechanism[2] (Table 2) makes such a comparison tenuous at best—the rate constants are well within the experimental errors of $\sim 10^{\pm 4}$ for k_1 and ≥5–7-fold for k_2-k_4.[2]

Table 2. Variation with Temperature of the Calculated Rate Constants (Observed via MacKinetics) for the Reduction of Pt(1,5-COD)Cl_2 via the Four-Step Mechanism of Scheme 1

temp (°C)	k_1 (h^{-1})	k_2 (× 10^3 M^{-1} h^{-1})	k_3 (× 10^3 M^{-1} h^{-1})	k_4 (× 10^3 M^{-1} h^{-1})
22.0	$\sim 10^{-5}$	2.7	0.040	0.32
30.0	$\sim 10^{-8}$	5.2	0.094	0.61
40.0	$\sim 10^{-6}$	8.1	0.32	2.1
50.0	$\sim 10^{-8}$	11	0.74	1.5
60.0	$\sim 10^{-11}$	16	1.4	3.2
70.0	$\sim 10^{-8}$	19	1.5	4.1
80.0	$\sim 10^{-7}$	28	2.0	4.1

Table 3. Variation with Temperature of the Calculated Rate Constants (Using Microcal Origin) in the Two-Step Mechanism of Scheme 2 for the Reduction of [Ir(1,5-COD)Cl]$_2$

temp (°C)	k_1 (h^{-1})	k_2 (× 10^3 M^{-1} h^{-1})
22.0	0.38(2)	5.8(2)
30.0	0.30(4)	5.8(5)
40.0	0.57(2)	3.0(1)
50.0	1.25(7)	9.0(5)
60.0	0.49(6)	10.7(7)
70.0	1.4(1)	4.3(6)
80.0	4.1(2)	12.8(8)

The rate constants in Table 3 for the two-step reduction of Ir^{I}, however, are more reliable, and therefore, Eyring plots can be constructed for the nucleation and growth steps. The plots (Supporting Information, Figure S12) give rare activation parameters for nucleation and growth, respectively, $\Delta H^{\ddagger}_1 = 15(1)$ kcal/mol and $\Delta S^{\ddagger}_1 = -14(1)$ eu, and $\Delta H^{\ddagger}_2 = 10(2)$ kcal/mol and $\Delta S^{\ddagger}_2 = -11(4)$ eu for [Ir(1,5-COD)Cl]$_2$. The activation parameters are similar to those found for the formation of $Ir^0_{\sim 300}$ nanoclusters from $(Bu_4N)_5Na_3[(1,5\text{-COD})Ir\cdot P_2W_{15}Nb_3O_{62}]$,[8a] $\Delta H^{\ddagger}_1 = 15(1)$ kcal/mol and $\Delta S^{\ddagger}_1 = -36(3)$ eu; $\Delta H^{\ddagger}_2 = 14(2)$ kcal/mol and $\Delta S^{\ddagger}_2 = -13(6)$ eu. Significantly, $\Delta H_{\text{nucleation}}$ is *not* much greater than ΔH_{growth},

(30) Huheey, J. E. *Inorganic Chemistry*, 3rd ed.; Harper & Row: New York, 1983; p A-51.
(31) Widegren, J. A.; Aiken, J. D., III; Özkar, S.; Finke, R. G. *Chem. Mater.* **2001**, *13*, 312.
(32) (a) Henglein, A.; Giersig, M. *J. Phys Chem. B* **2000**, *104*, 6767. (b) See footnote 4e of ref 31.
(33) Finney, E. E.; Ott, L. S.; Watzky, M. A.; Finke, R. G. "Transition-metal Nanocluster Formation Kinetic and Mechanistic Studies en Route to Size Control", manuscript in preparation.

Table 4. Variation of the Mechanism and Rate Constants vs Initial Concentration of Pt^{II} in the Reduction of Pt(1,5-COD)Cl_2

$[Pt^{II}]$ (mM)	k_1 (h^{-1})	k_2 ($\times 10^3$ M^{-1} h^{-1})[a]	k_3 ($\times 10^3$ M^{-1} h^{-1})[a]	k_4 ($\times 10^3$ M^{-1} h^{-1})[a]
0.3	$\sim 10^{-4}$	24	0.80	0.59
0.6	~ 0.2	13	5.0	32
0.9	$\sim 10^{-5}$	52	0.76	0.52
1.2	$\sim 10^{-7}$	45	1.1	9.6
2.4	$\sim 10^{-6}$	33	0.40	2.0
12.0	$\sim 10^{-2}$	1.4	0.46	0.15

[a] The values of k_2, k_3, and k_4 were each corrected as required by multiplying the observed rate constant by [cyclohexene]/[Ir], as described in a previous report.[8a]

Table 5. Variation of the Mechanism and Observed Rate Constants vs Initial Ir^I Concentration for the Reduction of [Ir(1,5-COD)Cl]$_2$

$[Ir^I]$ (mM)	k_1 (h^{-1})	k_2 ($\times 10^3$ M^{-1} h^{-1})[a]
0.3	0.28(2)	11.0(6)
0.6	0.68(3)	6.5(4)
0.9	0.62(7)	9.3(8)
1.2	0.82(4)	5.1(2)
2.4	0.92(5)	4.7(2)
12.0	6.0(5)	1.1(2)

[a] The values of k_2 were each corrected as required by multiplying the observed rate constant by [cyclohexene]/[Ir], as described in a previous report.[8a]

as previous literature has implied.[34] Note also that the negative entropy of the nucleation step, k_1, is evidence for its true higher-order $n\mathrm{A} \rightarrow \mathrm{A}_n$ ($=\mathrm{B}_n$) nature at least for Ir and as detailed elsewhere.[35]

Concentration Effects. These studies were carried out at 60 °C at concentrations of 0.3, 0.6, 0.9, 1.2, 2.4, and 12.0 mM Pt^{II}(1,5-COD)Cl_2 and [Ir^I(1,5-COD)Cl]$_2$ with no added ligands. As can be seen from the data (Table 4 for Pt and Table 5 for Ir), the mechanism does not change over the range of concentrations studied. The reduction of Pt^{II} follows the four-step mechanism over the range of 0.3–12.0 mM, and the reduction of Ir^I follows the two-step mechanism over the same concentration range. The greater error[1,2] in determining the four rate constants for the four-step mechanism, vs the better determined two-step rate constants, is one point obvious from comparing the data in Tables 4 and 5. The interesting concentration dependence of the k_1 and k_2 rate "constants" in Table 5 is at least partially understood but requires a more detailed treatment than is possible here. Hence, the required analysis and discussion will be provided elsewhere.[35]

Stirring Effects. The effects of stirring on transition-metal nanocluster synthesis have been studied, specifically the need to avoid H_2 gas-to-solution mass-transfer limitations resulting from insufficient stirring which will otherwise ruin nanocluster syntheses if present.[36] Therefore, in examining the effects of stirring on the mechanism, care must be taken to maintain catalyst-dependent (i.e., chemical reaction rate-limiting) kinetics so that the kinetics of nanocluster formation are what is being measured, not the mass transfer of gaseous H_2 into solution.

Table 6. Control Experiments Probing Any Variation of the Rate Constants in the Mechanism of Scheme 1 with Stirring Rate for the Reduction of Pt(1,5-COD)Cl_2

stirring rate (rpm)	k_1 (h^{-1})	k_2 ($\times 10^3$ M^{-1} h^{-1})	k_3 ($\times 10^3$ M^{-1} h^{-1})	k_4 ($\times 10^3$ M^{-1} h^{-1})
640	$\sim 10^{-11}$	16	1.4	3.2
1500	$\sim 10^{-6}$	16	1.4	4.1

Table 7. Control Experiments Probing Any Variation of the Rate Constants in the Mechanism of Scheme 3 with Stirring Rate for the Reduction of [Ir(1,5-COD)Cl]$_2$

stirring rate (rpm)	k_1 (h^{-1})	k_2 ($\times 10^3$ M^{-1} h^{-1})
640	0.42(8)	3.6(1)
1500	0.52(4)	4.1(6)

The rate of stirring used throughout this study was ~640 rpm. Reduction of (1,5-COD)$PtCl_2$ was carried out using a higher stirring rate, ~1500 rpm, to determine whether this faster rate would have an effect on the mechanism. Not only did the faster stirring rate *not* affect the mechanism, but the calculated rate constants themselves remained unchanged within experimental error (Table 6): the rate constants k_2-k_4 are nearly identical, and the k_1 values are within the known,[1,2] $10^{\pm 4}$ experimental error of k_1.

The same result was seen for the reduction of [Ir(1,5-COD)Cl]$_2$—the reduction follows the two-step mechanism at both of the stirring rates studied. The calculated rate constants k_1 and k_2 at both stirring rates are also the same within experimental error (Table 7). We note that these stirring rate controls are not trivial—both as done herein and for literature systems where they remain to be done—due to the documented large effects of mass-transfer limitations on nanocluster syntheses and other reactions with autocatalytic steps.[15b]

Effects of Changing Precursor Concentrations and Reaction Temperatures on the Product of the Reductions (Nanoclusters vs Bulk Metal). At this point we have shown that the reduction of Pt(1,5-COD)Cl_2 follows the four-step, double-autocatalytic mechanism over the concentration range of 0.3–12.0 mM (at a constant reaction temperature of 60.0 °C) and over the temperature range of 22.0–80.0 °C (using a constant Pt concentration of 0.6 mM). In previous reports[1,2] we showed that reduction of a 1.2 mM Pt(1,5-COD)Cl_2 solution in acetone at 22.0 °C gave only bulk Pt^0 metal, while reduction of a 0.6 mM solution in propylene carbonate at 60.0 °C gave Pt^0_n nanoclusters with no bulk metal present; both reductions followed the four-step mechanism. The question arises, then, of what factors (concentration, temperature, solvent) are significant in determining whether the major product is nanoclusters or bulk metal.

To answer this question, we considered to the products of the reductions under each set of conditions given in Tables 2−5. At every temperature studied using a 1.2 mM solution of Pt(1,5-COD)Cl_2 in propylene carbonate, bulk Pt^0 metal was the only observed product. This suggests that the reaction temperature has little or no effect on the reaction product (nanoclusters vs bulk metal) at a given metal concentration.

(34) (a) Turkevich, J.; Stevenson, P. C.; Hillier, J. *Faraday Discuss. Chem. Soc.* **1951**, *11*, 55. (b) Bullen, C. R.; Mulvaney, P. *Nano Lett.* **2004**, *4*, 2303.

(35) Note that, during the induction period so that [A] is effectively constant for $n\mathrm{A} \rightarrow \mathrm{A}_n$, rate constant k_1', where $1/nk_1'[\mathrm{A}]^n = k_1$ (for $\mathrm{A} \rightarrow \mathrm{B}$, rate constant k_1). That is, to a good first approximation, we can still use the $\mathrm{A} \rightarrow \mathrm{B}$ mechanism in the curve fits and even if the underlying mechanism is the higher-order $n\mathrm{A} \rightarrow \mathrm{A}_n$ ($=\mathrm{B}_n$), at least for Ir. See ref 33.

(36) Aiken, J. D., III; Finke, R. G. *J. Am. Chem. Soc.* **1998**, *120*, 9545.

The results of changing the concentration while keeping the temperature constant at 60 °C, however, are more complex. At concentrations of 0.3 and 0.6 mM in propylene carbonate, nanoclusters were the only observable product (i.e., no bulk metal was observed). At 0.9 and 1.2 mM, some bulk metal was observed in light gray solutions, indicating the presence of both nanoclusters and bulk metal in the reaction solution. At 2.4 mM, bulk metal was the only observed product. These results confirm that at a given temperature (e.g., 60 °C in the present case) the precursor concentration is one important variable in determining whether the final, observed product includes, or primarily is, bulk metal.

To further test the importance of the solvent (acetone vs propylene carbonate) on the observed products, a 0.6 mM solution of $[Ir(1,5\text{-COD})Cl]_2$ (containing 1.2 mM Ir) was reduced at 30 °C separately in acetone and in propylene carbonate. The reduction followed the two-step mechanism in both solvents; however, in acetone, bulk Ir^0 metal was the only observed product, while in propylene carbonate, a clear brown Ir^0_n nanocluster solution resulted with *no* black precipitate (no Ir^0 bulk metal present). Additionally, the reduction of $[Ir(1,5\text{-COD})Cl]_2$ in the presence of 5 equiv of pyridine was repeated in propylene carbonate. In acetone, a clear colorless solution with black precipitate resulted after cyclohexene hydrogenation was complete (see the kinetic curve in Figure 6). In propylene carbonate, however, a clear black solution was present along with some black precipitate. This black solution persisted for several hours after the reduction was complete, and TEM showed the presence of 5 ± 2 nm nanoclusters. We conclude, therefore, that the solvent (and in particular propylene carbonate) has a major influence on whether a nanocluster or bulk metal product is the final product of a reduction—presumably by effectively stabilizing and thus slowing the rate of agglomeration, even when the mechanism of agglomeration remains as the four-step mechanism. The effects can be subtle, and, again, nucleation is probably important since the solvent can also be a ligand. In addition, DLVO theory predicts that solvents with higher dielectric constants will be more stabilizing.[37] Finally, our previous, tentative conclusion that increasing temperature and decreasing concentration favors nanocluster formation[1,2] must be modified, therefore, to emphasize the role of the higher dielectric constant and, therefore, more stabilizing, solvents as the greater influence in favoring nanocluster preparations.

What is the Nature of B vs C? A second question that arises is: if a reduction that gives no bulk metal but large $Pt(0)_{\sim 2200}$ nanoclusters[1,2] follows the four-step mechanism, then what is the nature of C? That is, is C larger bulk-like (but still soluble) metal particles? If so, at what point does B (nanoclusters) become C (larger, apparently more bulk-metal-like particles)? To gain some insight into this question, we note that even when no visible bulk metal is present in the reduction of $Pt(1,5\text{-COD})Cl_2$ (i.e., when a clear brown solution with no black precipitate is the product of the reaction), the four-step mechanism, with C as the active hydrogenation catalyst, is necessary to fit the kinetic data. Therefore, C must include larger, closer to bulk-metal-like, but still soluble Pt^0_n particles. The Pt^0_n nanoclusters formed using the modified conditions of 0.6 mM and 60 °C in propylene carbonate without added ligand are 7 ± 3 nm by TEM (Supporting Information, Figure S13); this is consistent with the four-step mechanism's prediction of larger particles being formed as the final product. However, the point at which nanoclusters (B) change to C (i.e., how large B must get before they become C) remains an open question that will require further study. EXAFS, XANES, and SAXS experiments are in progress.[3]

Comment on the Observation of Two-Step Kinetics Yet Bulk Metal as the Observed Product. Another important observation and associated question not yet addressed is "how can bulk metal be the (final) product when the two-step mechanism fits the kinetic data?" The primary answer here is apparent if one looks at the times at which bulk metal forms when two-step vs four-step mechanism fits to the kinetic data are seen (Table 1). When the two-step mechanism is followed, bulk metal is observed *after* the cyclohexene hydrogenation is complete. That is, metastabilized nanoclusters, B, are formed and are the main species present while the cyclohexene hydrogenation reporter reaction is operative. Agglomeration still occurs, undoubtedly via the k_3 and k_4 pathways, but after the kinetics are completed; hence, the k_3 and k_4 steps are not detected.

On the other hand, when the four-step mechanism is followed, bulk metal is observed to form at the end of the induction period (vide supra). Thus, the cyclohexene hydrogenation reaction reports the formation of both the nanoclusters, B, and their agglomeration to C. Overall, it is again apparent, however, that spectroscopic studies directly monitoring B, C, and bulk metal vs time would be valuable studies that need to be undertaken.[3]

Effect of the Four-Step Mechanism on Nanocluster Size and Size Distribution and the Relationship between the k_3 and k_4 Steps to "Ostwald Ripening". When nanoclusters are formed via the four-step mechanism, the final sizes are larger and of broader dispersity than those seen for formed via the two-step mechanism. For example, the average size of the polyoxoanion-stabilized $Ir^0_{\sim 300}$ nanoclusters formed by the two-step mechanism is 22 ± 3 Å,[8] corresponding to $\pm \leq 15\%$ (so-called "near-monodisperse" clusters[38]), while Ir^0_n nanoclusters formed from $[Ir(1,5\text{-COD})Cl]_2$ in the presence of pyridine and by the four-step mechanism average 5 ± 2 nm, or a polydisperse $\pm 40\%$. Other factors may be at play in the size and size distributions of the nanoclusters, including ligands or solvent, but on the basis of these results, the four-step mechanism provides a mechanism-based rationale for the "size refocusing" of nanoclusters that is mentioned in the literature,[39] in which agglomeration of clusters causes a widening ("defocusing") of the size distribution. Historically, size refocusing has generally been attributed to Ostwald ripening, in which larger particles grow at the

(37) Ott, L. S.; Finke, R. G. *Coord. Chem. Rev.* **2007**, *251*, 1075.

(38) Finke, R. G. In *Metal Nanoparticles: Synthesis, Characterization and Applications*; Feldheim, D. L.; Foss, C. A., Jr., Eds.; Marcel Dekker: New York, 2002; Chapter 2.

(39) (a) Peng, X.; Wickham, J.; Alivisatos, A. P. *J. Am. Chem. Soc.* **1998**, *120*, 5343. (b) Rogach, A. L.; Talapin, D. V.; Shevchenko, E. V.; Kornowski, A.; Haase, M.; Weller, H. *Adv. Funct. Mater.* **2002**, *12*, 653.

Scheme 4

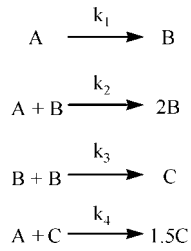

expense of smaller particles. The difference between the mechanism presented herein and Ostwald ripening is that in the present mechanism no particle dissolution is assumed to take place; rather, two nanoclusters (B) agglomerate to form a larger cluster (C). Overall, it seems likely that our k_3 and k_4 steps are an intimate part of what has been loosely called "Ostwald ripening" in the literature.

Exclusion of Three Additional Alternative Mechanisms. Previously, 15 alternative mechanisms were experimentally excluded on the basis of alternative fits of the data for Pt(1,5-COD)Cl_2 reduction in the presence of Proton Sponge and Bu_3N.[2] We have tested three more alternative mechanisms: a mechanism that replaces the second step in Scheme 1 with A + B + B → 3B; a mechanism that includes an equilibrium between A + B and a complexed [AB] species; and a mechanism that excludes the autocatalytic growth step A + B → 2B from Scheme 1. None of these mechanisms fit the experimental data well. (The attempted fits are given in the Supporting Information, Figure S14.) In short, we have been able to rule out a total of 18 other mechanisms en route to providing strong support for the four-step mechanism in Scheme 1.

Testing the Alternative, A + C → 1.5C Double-Autocatalytic Mechanism. Previously, it was found that a different autocatalytic mechanism fit equally well the cyclohexene-loss curves for the reduction of Pt(1,5-COD)Cl_2 shown in Figure 1.[1,2] This second mechanism simply replaces the final B + C → 1.5C step of the four-step mechanism (Scheme 1) with A + C → 1.5C (Scheme 4) (i.e., this mechanism assumes that bulk metal, C, is the dominant catalyst for the reduction of the precursor, A, as well as for the hydrogenation of cyclohexene).[2]

In order to distinguish the two mechanisms, the reaction was followed by GLC in our prior work[1,2] to gain more direct (albeit less precise) data by following the evolution of cyclooctane from reduction of the 1,5-COD in the Pt(1,5-COD)Cl_2 precursor. The resultant rate constants calculated from the GLC data are within the range of those calculated from cyclohexene loss data when both data sets were fit by the four-step mechanism in Scheme 1, but *not* when both data sets were fit by the alternative mechanism with the conceivable A + C → 1.5C step.[1,2] That is, the dominant mechanism for reduction of Pt(1,5-COD)Cl_2 is that provided back in Scheme 1 with B + C → 1.5C as the fourth, second autocatalytic step.

We also wondered whether Scheme 4, with its A + C → 1.5C step, provides a better or worse fit to the data in Figure 5 for the reduction of [Ir(1,5-COD)Cl]$_2$ with 5 equiv of pyridine. The mechanism in Scheme 4 gave a fit that was visually as good as that for the mechanism in

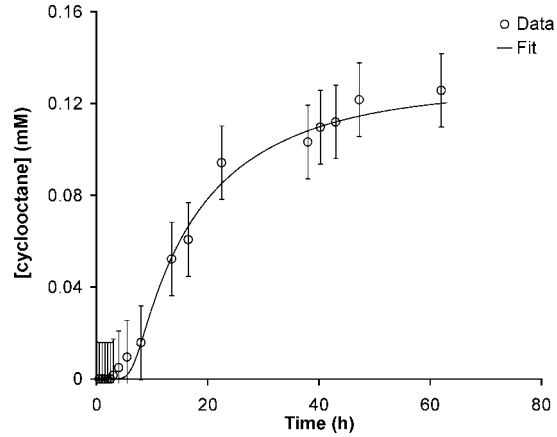

Figure 11. Direct measurement of cyclooctane evolution for the reduction of [Ir(1,5-COD)Cl]$_2$ with 5 equiv of pyridine. The data are well fit to the double-autocatalytic mechanism given in eq 1 with C as the catalyst and with B + C → 1.5C as the fourth step of the mechanism. The calculated rated constants fall within the range of values obtained via the cyclohexene reporter reaction (see Figure 5), giving strong support to the hypothesis that the reduction indeed follows the four-step mechanism given in Scheme 1 (with B + C → 1.5C and not A + C → 1.5C, as the fourth step of the mechanism). $k_1 \approx 3 \times 10^{-3}$ h^{-1}; $k_2 \approx 830$ M^{-1} h^{-1}; $k_3 \approx 37$ M^{-1} h^{-1}; $k_4 \approx 69$ M^{-1} h^{-1}; residual = 0.024.

Scheme 1 with the B + C → 1.5C step (Supporting Information, Figure S15). Therefore, we performed the GLC study on this [Ir(1,5-COD)Cl]$_2$ + 5pyridine system as well—it is well-known that changing reaction conditions can (sometimes dramatically) change reaction mechanisms in transition-metal chemistry.[40] The rate constants derived from the cyclooctane data (Figure 11) fall within the range of those derived from the cyclohexene data when both data sets were fit by the B + C → 1.5C mechanism; this is not the case for the A + C → 1.5C mechanism (Supporting Information, Figure S16). Therefore, the dominant mechanism for the reduction of [Ir(1,5-COD)Cl]$_2$ with 5 equiv of pyridine is, again, the B + C → 1.5C mechanism of Scheme 1. (As noted before,[2] we cannot exclude some contribution by the A + C → 1.5C mechanism.)

Three Literature Systems Which Follow the Four-Step Mechanism: Further Evidence for the Greater Generality of the Four-Step Mechanism. We have found three additional nanocluster preparations that follow the four-step, double-autocatalytic mechanism. The first was described previously;[1] it is the reduction of $H_2PtCl_6 \cdot 6H_2O$ in the presence of poly(vinylpyrrolidone) in methanol. The step-function-like kinetics of that reduction were best fit by the four-step mechanism (although the formation of bulk Pt(0) metal in that system appears to compromise the fit somewhat).[41] Under different conditions, we have also seen a two-step mechanism for H_2PtCl_6 reduction.[41]

Looking back at our own literature revealed another example of the four-step mechanism. In 2002, a study in

(40) See for example: Nappa, M. J.; Santi, R.; Halpern, J. *Organometallics* **1985**, *4*, 34. In this case, reactions of $RMn(CO)_4L$ with $HMo(CO)_4L$ proceed by different mechanisms depending on the solvent, concentration of CO, and identity of L. The present work also makes this point, but now in transition-metal nanocluster chemistry, showing that addition of ligands changes the nanocluster formation and agglomeration mechanisms.

(41) Mondloch, J.; Finney, E. E.; Yan, X.; Finke, R. G. Manuscript in preparation.

our laboratories ranked common anionic nanocluster stabilizers.[42] One of those stabilizers ranked was the citrate ion, $C_6H_5O_7^{3-}$. Reduction of the solvated iridium complex $[Ir(1,5\text{-}COD)(CH_3CN)_2]^+[BF_4]^-$ in the presence of 1 equiv each of $[Bu_4N]_3[C_6H_5O_7]$ and Bu_4NOH gave a kinetic curve with a sudden "turn-on" and no inflection point, the two visual signs that the four-step mechanism is in operation (see Figure S8 of the Supporting Information[42]). Fitting the data originally in that figure demonstrates that the four-step mechanism fits the Ir(1,5-COD)$^+$/citrate^{3-} system (Figure S17 of the Supporting Information).

One more observation of the four-step mechanism comes from the work of Scheeren et al. using PtO_2 clusters to hydrogenate cyclohexene in ionic liquids.[43] The formation and catalysis of those clusters also follows the same four-step mechanism depending on reaction conditions as demonstrated by the fits provided elsewhere,[43] which employ the four-step mechanism.[1,2]

Conclusions

Herein we have shown the following:

• The four-step, double-autocatalytic mechanism discovered previously[1,2] for the reduction of the platinum salt Pt(1,5-COD)Cl_2 is more general to the reduction of the analogous salts of Ru^{II}, Ir^{I}, Rh^{I}, and Pd^{II} (and thus presumably other metals) in the presence of appropriate ligands and under the conditions examined.

• The features of the four-step mechanism are seen in three additional cases of transition-metal reduction from the literature, further evidence for the greater generality of the four-step mechanism.

• The main factors that decide what mechanism will be followed are the metal, the ligands that are present (in particular, the metal–ligand bond energy), and the amount of ligand.

• One main effect of added ligand appears to be the slowing of the k_1, nucleation step. This, in turn, leads to fewer, but larger, nanoclusters and thus more agglomeration. An underlying, controlling effect appears to be the change of M_n−ligand bond energy with nanocluster size (i.e., with changing n value): added ligands bond more tightly to small nanoclusters, decreasing k_1, while larger nanoclusters with weaker M_n−ligand bonds can still undergo agglomeration by either the k_3 and/or k_4 pathways.

• The number of steps in the mechanism seems to be unaffected by changes in metal concentration, temperature, stirring rate, and solvent, at least within the ranges studied.

• However, the solvent used does influence the final products of the reductions, higher dielectric solvents (such as propylene carbonate[37]) favoring the formation of nanoclusters over bulk metal.

• The activation parameters for nucleation and growth are rather similar to one another, as was found for polyoxoanion-stabilized Ir^0 nanoclusters, in contrast to implications of previous literature that nucleation should have a larger $\Delta H^{\ddagger}$.[34]

• Both the size and size distribution of the nanoclusters are larger when the four-step mechanism is followed, as the mechanism predicts.

• The alternative mechanism in which the metal product C catalyzes the reduction of precursor A is not a major contributor for the reduction of either Pt(1,5-COD)Cl_2 or $[Ir(1,5\text{-}COD)Cl]_2$, the latter in the presence of pyridine.

• The true nature of products B and C need to be investigated in more detail by EXAFS, XANES, SAXS, and other appropriate methods in order to intimately characterize the products and to determine at what point B effectively becomes C.[3]

Overall, the present work demonstrates that the four-step mechanism should be considered any time a transition-metal salt is reduced to form nanoclusters and curves like those in Figures 1, 3, 5, 6, 7, 8, or 10 are seen. The present work also provides considerable additional insight into the four-step, double-autocatalytic mechanism. Since the four-step mechanism is, in the end analysis, the "Ockham's razor" (i.e., minimalistic) mechanism of "just" nucleation (autocatalytic) growth, (bimolecular) agglomeration, and a second type of (autocatalytic) agglomeration, it seems likely that the four-step mechanism[1,2] may well prove to be much more general. Time will tell.

Acknowledgment. We thank Professors Irving R. Epstein at Brandeis University and James D. Martin at North Carolina State University for their suggested alternative mechanisms shown in Figure S14 of the Supporting Information and Professor Thomas Meersman at CSU for his suggestion to use the *F* test in discerning data sets. Support from DOE Grant DE-FG02-03ER15453 is gratefully acknowledged.

Supporting Information Available: Experimental procedure for the synthesis of the solvated metal complexes $[Ir(1,5\text{-}COD)(CH_3CN)_2]^+[BF_4]^-$ and the previously unreported rhodium solvate complex $[Rh(1,5\text{-}COD)(CH_3CH)_2]^+[BF_4]^-$; preparations of the solvated complexes $[Pt(1,5\text{-}COD)Cl(CH_3CN)]^+[BF_4]^-$ and $[Pd(1,5\text{-}COD)Cl(CH_3CN)]^+[BF_4]^-$; pressure oscillations in reductions carried out at 80 °C; two- and three-step mechanism fits to the data for the reduction of Pt(1,5-COD)Cl_2 in the absence of ligand; kinetic curve for the reduction of $[Ir(1,5\text{-}CODCl]_2$ in the presence of 1 equiv of pyridine; kinetic curves for the reduction of $[Ir(1,5\text{-}COD(CH_3CN)_2]^+[BF_4]^-$ in the absence of ligand and in the presence of 1 equiv of pyridine, 1 and 2 equiv of Bu_4NCl; kinetic curves for the reduction of $[Rh(1,5\text{-}COD)(CH_3CN)_2]^+[BF_4]^-$ in the absence of ligand and in the presence of 80 equiv of pyridine, 1 and 2 equiv of Bu_4NCl, and 10 equiv of 4-(dimethylamino)pyridine; reduction of Pd(1,5-COD)Cl_2 in the presence of 4-(dimethylamino)pyridine, 1,10-phenanthroline, and octanethiol; an alternate explanation for the difference between the reductions of $[Ir(1,5\text{-}COD)Cl]_2$ and $[Rh(1,5\text{-}COD)Cl]_2$ in the presence of pyridine, including TEM images of nanoclusters formed from the reductions of $[Ir(1,5\text{-}COD)Cl]_2$ and $[Rh(1,5\text{-}COD)Cl]_2$; four-step mechanism fit of the kinetic data for the reduction of Pd(1,5-COD)Cl_2 in the absence of ligand; control experiments showing that the change in solvent from acetone to propylene carbonate has no effect on the number of mechanistic steps; Eyring plots for the nucleation and growth of Pt and Ir nanoclusters; TEM of Pt^0_n nanoclusters formed from the reduction of a 0.6 mM solution of Pt(1,5-COD)Cl_2 at 60.0 °C; attempted fits of three additional alternative mechanisms for the reduction of Pt(1,5-COD)Cl_2; fitting the

(42) Özkar, S.; Finke, R. G. *J. Am. Chem. Soc.* **2002**, *124*, 5796.
(43) Scheeren, C. W.; Domingos, J. B.; Machado, G.; Dupont, J. *J. Phys. Chem. B* **2006**, *110*, 13011.

cyclooctane evolution data for the reduction of $[Ir(1,5\text{-COD})Cl]_2$ with 5 equiv of pyridine to the alternative A + C → 1.5C mechanism (cyclohexene loss and cyclooctane evolution data); fit to the four-step mechanism of the reduction of $[Ir(1,5\text{-COD})(CH_3CN)_2]^+[BF_4]^-$ in the presence of 1 equiv each of tetrabutylammonium hydroxide and tetrabutylammonium citrate; table comparing *F* values for the two- and four-step mechanisms for the reduction of $Pt(1,5\text{-COD})Cl_2$, $Ru(1,5\text{-COD})Cl_2$, and $[Ir(1,5\text{-COD})Cl]_2$ in the presence of 1 equiv of Bu_4NCl and 5 equiv of pyridine, $[Rh(1,5\text{-COD})Cl]_2$ in the presence of 1 equiv of Bu_4NCl and 10 equiv of 4-(dimethylamino)pyridine. This information is available free of charge via the Internet at http://pubs.acs.org.

CM071088J